Analysis of Various Parameters Affecting Signals in Resting-state Mouse Brain Photoacoustic Microscopy: a Simulation Study

H. Ghadiri, M. R. Fouladi
Medical Physics and Biomedical Engineering Department
Research Center for Molecular and Cellular Imaging
Tehran University of Medical Sciences
Tehran, Iran

A. Rahmim
Radiology and Radiological Sciences Department
Johns Hopkins University
Baltimore, USA

Abstract—**Photoacoustic imaging is an emerging modality which is being developed due to its high capabilities. At the other hand, one of the most interesting areas of research is brain imaging. Photoacoustic imaging has been used in brain imaging due to its capability of both functional and anatomical imaging. Photoacoustic spectral analysis is one of the last research areas in this field. But, as our point of view, only looking to frequency components of photoacoustic signals doesn't make all available required data. Thus, in this work, our study presents both time-domain and frequency-domain analysis of photoacoustic signals and demonstrates that going deeper through the brain will decrease contrast and resolution of photoacoustic microscopy system for imaging of resting-state mouse brain vasculature and this can be solved by using an exogenous contrast agent like Indocyanine Green. Also, by using analysis of photoacoustic signals, we demonstrated that Indocyanine Green will increase both depth resolution and contrast. Also, simulations and analysis done on different sizes of hemoglobin absorber containers demonstrated that there is a need to ultra-broadband transducers for reaching more precise analysis of photoacoustic signals, and this means Acoustic-Resolution Photoacoustic Microscopes are less efficient for being used for spectral analysis.**

Keywords—photoacoustic microscopy; PASA; mouse brain; simulation; Indocyanine Green

I. INTRODUCTION

Photoacoustic Imaging (PAI) is a non-ionizing hybrid medical imaging modality based on photoacoustic effect which was described by Alexander Graham Bell at 1880 for the first time [1]. Briefly, a pulsed laser beam illuminates the tissue, then absorption of photons, reaching the Region Of Interest (ROI), leads to a slight localized heating of the tissue causing thermoelastic expansion and generating pressure waves, which can be detected by ultrasound transducer(s) as photoacoustic (PA) signals. PAI benefits from optical contrast and ultrasound resolution simultaneously that means more depth resolution than pure optical imaging techniques and more contrast rather than ultrasound imaging techniques, though the origins of contrast are completely different.

PAI like other medical imaging modalities has contrast agents, either endogenous or exogenous. Hemoglobin, melanin, lipids, collagen, elastin and water are some endogenous agents studied. A variety of exogenous agents have been used by researchers (e.g. Indocyanine Green (ICG), Evans Blue, IRDye800, Quantum Dots, copper sulfide nanoparticles) [2-5]. During the last decade, PAI has found many clinical applications in fields like urology, dermatology, gynecology, hematology, ophthalmology and specifically brain imaging [6-7].

Capability of this modality in both anatomical and functional imaging has made it an opportune method for brain imaging. Studies on brain of small animals like mouse have measured quantities like Cerebral Metabolic Rate of Oxygen ($CMRO_2$) and Saturation of Oxygen (sO_2) either with or without use of exogenous agents. Earlier, various systems have been used by researchers of this emerging field, among them; Photoacoustic Microscopy (PAM) and Photoacoustic Tomography (PAT) have found major applications. Focused spherical, ring-shaped transducers or rotational multi-element transducers have been used in PAT. Transducers, using different techniques of focusing, detect signals of various ROIs in tissues and then reconstruction of acquired PA signals forms tomographic images. PAM systems are confocal microscopes which based on their instrumentation can be divided into two fields; Optical-Resolution Photoacoustic Microscopy (OR-PAM) or Acoustic-Resolution Photoacoustic Microscopy (AR-PAM). Briefly, the focus of pulsed laser beam in OR-PAM is narrow and a broadband ultrasound transducer is used for sensitive detection of waves with broad range of frequencies. In contrast, AR-PAM utilizes narrower bandwidth transducers and the focal spot of laser light is broader at the focal zone of microscopy [8-11].

ICG is one of the most important agents used in photoacoustic brain imaging. It is a non-toxic agent with suitable clearance which can be transmitted across Blood-Brain Barrier and has an absorption peak at ~800nm. Wavelengths between 700-1064nm are in Near Infrared (NIR) range of optical spectrum that light penetration achieves its maximum level, that's why almost all agents are made with optical absorption peak in wavelengths in NIR region [4].

A majority of previous studies on PAI were focused on instrumentation, different imaging techniques (e.g. PAM, PAT) and implementation of novel reconstruction algorithms etc. Recently, a new technique termed Photoacoustic Spectral Analysis (PASA) is being developed. The major purpose of

978-1-5090-5820-4/16/$31.00 ©2016 IEEE

PASA is quantification of different characteristics of tissues and biological microstructures [12-13].
Earlier studies like spectral analysis of PAI data from prostate adenocarcinoma tumors in a murine model have focused on morphological characterization of biological tissues only by implementing frequency-domain analysis [14].
In this work, a simulation study presents, for the first time to the best of our knowledge, both time-domain and frequency-domain analysis of PA signals generated by different concentrations of ICG and comparing with signals generated by Hemoglobin in resting-state mouse brain using narrowband focused ultrasound transducer. In addition, analysis of PA signals from different imaging depths and different sizes of absorbers augments our study. Although, using AR-PAM system which is similar to our simulation setup hasn't been reported so far.

II. Materials and Methods

A. Theory

When pulsed laser illuminates the mouse brain, light propagates through the medium and experiences several interactions; mainly scattering and absorption. A general model of light propagation through scattering media is described by Boltzmann equation which is known as Radiative Transfer Equation (RTE) in our model. Boltzmann equation in the steady state can be written as (1) with supplementary equation (2)

$$(\hat{s}.\nabla + \mu_t(r))\varphi(r,\hat{s}) = \mu_s(r)\int_{S^{n-1}} \Theta(\hat{s},s')\varphi(r,s')d\hat{s}' + q(r,s') \quad (1)$$

$$\mu_t(r)=\mu_s(r) + \mu_a(r) \quad (2)$$

Here $\mu_t(r)$, $\mu_s(r)$ and $\mu_a(r)$ are attenuation, scattering and absorption coefficients in the units of per meter, respectively. $\varphi(r,\hat{s})$ is the number of photons per unit volume at position r in angular direction of velocity $\hat{s}$ in the units of per cubic meters per stradian. $q(r,\hat{s})$ is the number of source photons and $\Theta(\hat{s},s')$ is the normalized phase function corresponding to the probability of scattering from direction $\hat{s}'$ to $\hat{s}$.
Absorption of photons slightly heats the medium; then thermoelastic expansion generates pressure waves, this is described by Morse and Uno Ingard, Diebold and colleagues as (3)

$$\nabla^2 p(r,t) - \frac{1}{v_s^2}\frac{\partial^2}{\partial t^2} p(r,t) = -\frac{\beta}{C_P}\frac{\partial}{\partial t} H(r,t) \quad (3)$$

Here $p(r,t)$ is the pressure wave in units of Pascal, v_s is the sound speed in units of meters per seconds, β is the isobaric volume expansion coefficient in units of per Kelvin, C_P is the isobaric specific heat and $H(r,t)$ is the thermal energy deposited by laser illumination at position r and time t. if thermal and stress confinement conditions be met, under illumination of a pulsed laser; the temporal component of $H(r,t)$ can be treated as a delta function and one can approximate (4)

$$H(r,t) \approx A(r)\,\delta(t) \quad (4)$$

Here $\delta(t)$ is delta function and $A(r)$ is absorbed energy density at position r that is (5)

$$A(r) = \int_{S^{n-1}} \varphi(r,\hat{s})d\hat{s} \quad (5)$$

Equation (5) can be calculated by using (1) and (2) under confinement conditions and then initial pressure P_0 generated at time $t=0$ and position r, described by Wang, is (6)

$$P_0 = \Gamma\, A(r) \quad (6)$$

Where Γ is Grüneisen parameter (dimensionless) and can be calculated by all defined parameters as (7)

$$\Gamma = \beta v_s^2/C_P \quad (7)$$

Thus, for running a simple simulation, there is a need to absorbed energy density $A(r)$ and Grüneisen parameter Γ. As we described, for calculating $A(r)$ we need to solve RTE, different solutions of this equation have been done in literature; using diffusion approximation, implementing Finite Element Method or Monte Carlo simulations. Despite considered methods, we used Neumann-series approach, described by Abhinav. K. Jha and colleagues. Thus, results shown in Fig.2 have been used. Also, results of Neumann-series approach for RTE solution are compared with MC simulation in this figure [15].
Note that transmitted flux F is calculated by $F(r)=A(r)/\mu_a$.
We used k-space method, described by Treeby and Cox, for simulation of PA wave propagation. Thus, K-Wave toolbox and MATLAB have been used for both simulation of PA wave propagation and spectral analysis of acquired PA signals.

B. Simulation

A pulsed laser with pulse duration of 5 ns at wavelength of 800 nm with initial energy flux of 31.7 mJ/cm^2 illuminated the mouse brain from the distance of 0.25 mm. Maximum Permissible Exposure (MPE) on skin should follow ANSI standard which for pulsed lasers in the wavelengths in the range of 700-1050 nm is written as (8)

$$MPE = 20\times 10^{2(\lambda-700)/1000}\, mJ/cm^2 \quad (8)$$

And at wavelength λ=800 nm of our simulation we have MPE=39.7 mJ/cm^2 that we use this value as our initial laser flux. Meanwhile, Grüneisen parameter has been assumed 0.8 as an average value for resting-state mouse brain [16].
We have used a concave focused sensor, focusing at different depths of P_0 generation, as ultrasound transducer. It consists of 97 point sensors which we have summed pressure data and averaged over 97 sensors for our measurements. The maximum supported frequency of our transducer is 3 MHz and it is a section of a sphere with radius of 1.4 mm.
The pulsed laser and concave sensor are confocal and the bandwidth of our simulated transducer is as low as possible, as we discussed, this setup is similar to AR-PAM setups.
We have used a mathematical mouse brain phantom. A sphere with a radius of 5 mm as mouse head, the skull with uniform thickness of 0.5 mm and brain tissue with radius of 4.5 mm have been simulated. Fig.1 shows our numerical phantom with spatial resolution of 230 μm and focused concave transducer used in our study.

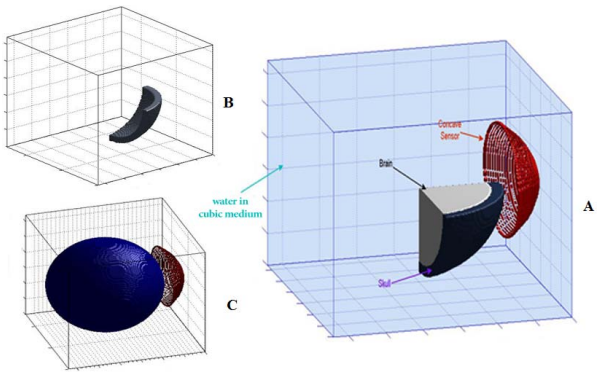

Figure 1: Mouse Brain phantom and focused sensor used in simulation.

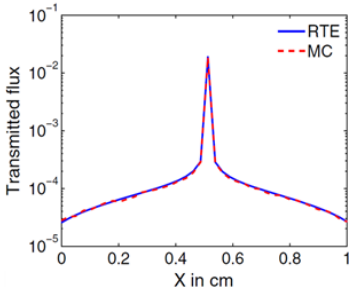

Figure 2: Neumann-series approach for RTE solution [15].

Table1: Acoustical and Optical properties of simulated materials.

	Attenuation Coefficient dB/MHz.cm	**Sound Speed m/s**	**Density g/cm^3**	**Extinction Coefficient ε (cm^{-1}M^{-1})**
Water	0.002	1480	1	-
Skull	20	4180	190	-
Brain	0.8	1550	103	-
Hemoglobin	-	-	-	816
ICG	-	-	-	154550

The materials used in the simulation were water, skull, brain, Hemoglobin and ICG, which their required optical and acoustical properties, used in simulation, are listed in table 1.
At the first level, we have acquired signals from spherical absorbers containing Hemoglobin with radiuses of 234 µm, 468 µm, 702 µm and 936 µm with a constant laser flux.
At the second level, we have acquired signals from ICG concentrations of 0.5 mg/L, 0.5, 5, 50, 100, 150 and 200 g/L.
At the third level, we have acquired signals from Hemoglobin at depths of 0.6 mm, 0.8 mm and 1 mm under internal surface of the mouse skull (i.e. 1.1 mm, 1.3 mm and 1.5 mm under the external surface of the mouse head).

C. *Analysis of PA Signals*

We didn't consider the term "analysis" just dedicated to frequency-domain analysis and Power Spectral Density (PSD) measurement. In addition, we discuss about time-domain PA signals.
Time-domain Analysis: we have measured and compared all peak-to-peak pressures (PPP) of PA signals at the transducer position. We assumed that transducer would detect PPP and changes it into voltage with a high sensitivity, and then it can be amplified. Simply, PPP can be calculated as following (9)

$$PPP(r_0) = P_{max}(r_0) - P_{min}(r_0) \quad (9)$$

Frequency-domain Analysis: we have done discrete-time Fourier transformation with Fast Fourier Transform (FFT) algorithm which is described by details in literature. Also, PSD of acquired signals in required situations are estimated.

Theoretically, scaling the magnitude squared of the discrete-time Fourier transform of acquired signal results an estimate of PSD; if we assume $p(r_0,n\tau)$ as acquired signal at transducer position r_0 and in n-th time step of simulation with pulse duration of τ=5ns, then we have (10)

$$PSD(f) = \frac{1}{(t_{end})F_S}\left|\sum_{n=0}^{t_{end}-1} p(r_0, n\tau)e^{-2\pi i fn/F_S}\right|^2 \quad (10)$$

Where F_S is sampling frequency of discrete-time Fourier transform and t_{end} is the last time step of simulation which changes during different circumstances and a typical value can be 10 micro-seconds.

III. RESULTS

A. *Analysis of PA Signals from Different Sizes of Hemoglobin*

Fig. 3, Fig.4 and Fig.5 are results of analysis of PA signals from Hemoglobin with radiuses of 234 µm, 468 µm, 702 µm and 936 µm.

B. *Analysis of PA Signals from Different Concentrations of ICG*

Fig.6, Fig.7, Fig.8 and Fig.9 are results of analysis of PA signals from ICG concentrations of 0.5 mg/L, 0.5 g/L, 5 g/L, 50 g/L, 100 g/L, 150 g/L and 200 g/L.

C. *Analysis of PA Signals from Different Depths of Microscopy*

Fig. 10, Fig.11 and Fig.12 are results of analysis of PA signals from depths of 1.5 mm, 1.3 mm and 1.1 mm.

IV. DISCUSSION

A. *Effects of Different Sizes of Hemoglobin on PA Signals*

Hemoglobin absorber containers of 234, 468, 702 and 936 micro-meter sizes have been studied in an equal depth (1.5 mm) and equal concentration (150 g/liter in plasma of blood) of mouse brain vasculature. Fig.3 shows time-domain PA signals of various sizes; obviously, one can see that the time of maximum pressure is increasing when size increases and this can lead us to a real-time PAM of smaller absorbers. Fig.4 shows that when the size of spherical hemoglobin containers increases, an increase in PPP can be seen. This mean with increasing size of microscopy field we can reach stronger PA signals, though in reality; when size increases other PA sources like subcutaneous melanoma will appear. Fig.5 is PSD of PA signals; this figure shows us when size of microscopy field decreases the center frequency of detected PA signals will increase and this means imaging of smaller objects can be done using broadband ultrasound transducers much well, although we have gone through this problem. Another peak about frequency of 1.75 MHz in graph of 234 µm absorber in power spectrum of Fig.5 shows that if we could increase maximum supported frequency of our detection system we could see more peaks about higher frequencies and this shows

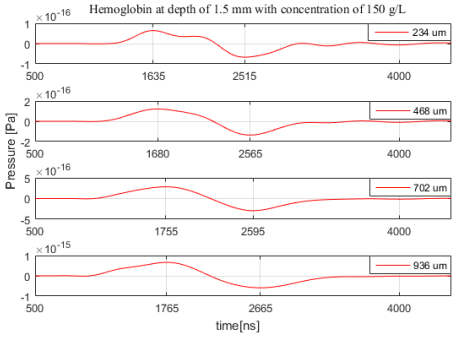

Figure 3: PA signals of Hemoglobin from depths of 234,468,702 and 936μm. The sensing time increases with increasing size.

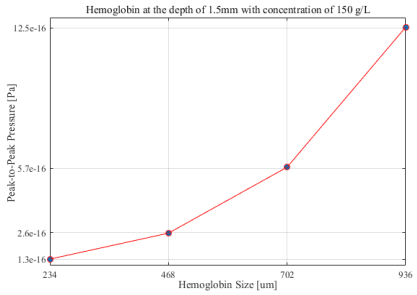

Figure 4: graph of Hemoglobin size to PPP; with increasing size, PPP increases too.

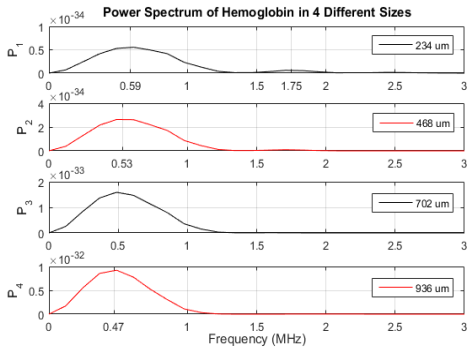

Figure 5: Power Spectrum of Hemoglobin in different sizes; existence of higher frequencies in P_1 is obvious when absorber size decrease.

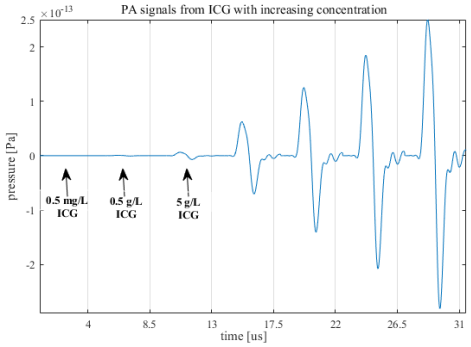

Figure 6: time-domain PA signals from different concentrations of ICG.

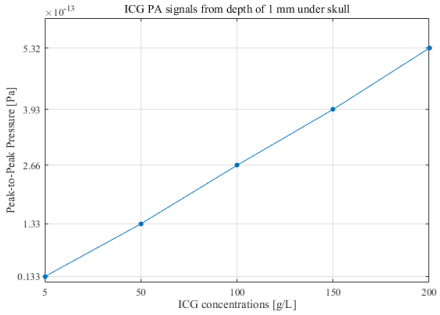

Figure 7: graph of ICG concentration to PPP.

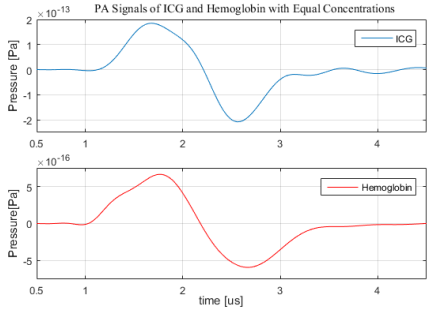

Figure 8: a comparison between time-domain PA signals from similar concentrations of Hemoglobin (red) and ICG (blue).

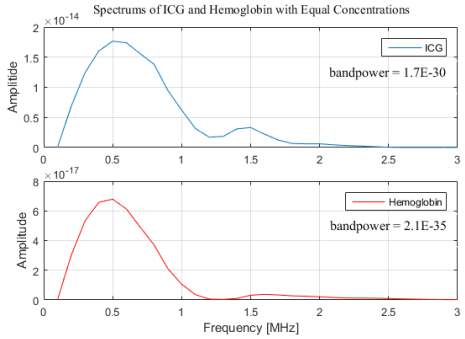

Figure 9: Power Spectrums of ICG (blue) and Hemoglobin (red) with equal concentrations. Their bandpowers are indicated too.

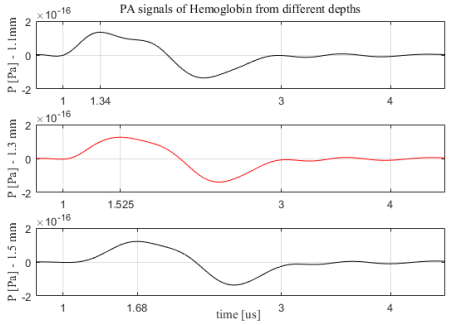

Figure 10: PA signals of Hemoglobin from depths of 1.1 mm, 1.3 mm and 1.5 mm under the surface of mouse head. The shortest depth has a faster pressure amplitude maximum.

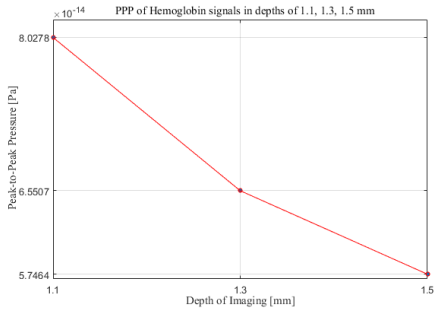

Figure 11: decreasing of PPP due to increasing the PAM depth.

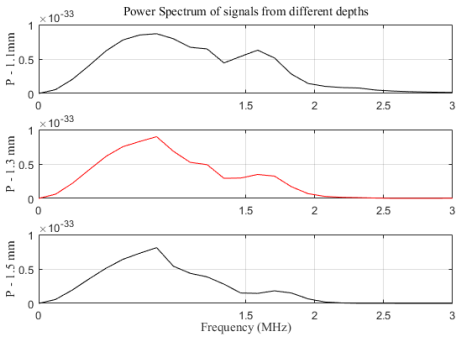

Figure12: Power Spectrums of PA signals from depths of 1.1mm, 1.3mm and 1.5mm under the surface of mouse head.

the nature of broadband PA signals; this phenomena wasn't seen in larger absorbers.

B. Effects of Different Concentrations of ICG on PA Signals

ICG concentration affects optical absorption coefficient, then P_0 will increase and with higher concentrations of ICG in brain vasculature we can detect stronger waves at the position of transducer, which is seen in Fig.6, showing that concentrations of 0.5 mg/L, 0.5 and 5 g/L couldn't be detected, because technology hasn't been developed as well as producing transducers with sensitivity of about 10^{-17} V/Pa. Fig.7 shows a linear increase in PPP with increasing concentration of ICG which can be measured with $F(r)$, P_0, depth and acoustic attenuation of mouse brain.

Fig.8 and Fig.9 show differences between PA signals of equal concentrations of Hemoglobin and ICG in time-domain and frequency-domain, respectively. Fig.8 shows that PA signal amplitude of ICG with 150 g/L concentration is 1000 times stronger than PA signal amplitude of the same concentration of Hemoglobin. Fig.9 shows when PA signal amplitude increases then bandpower of PSD increases. Also, another peak about higher center frequency shows capability of ICG in making greater spatial resolutions for PAM systems, in addition to its contrast enhancement.

C. Effects of Different Depths of Microscopy on PA Signals

Fig.10 indicates that when depth of microscopy increases signal acquisition time will increase; this means that going through deeper tissues in mouse brain costs as losing time and corrupting real-time capability of PAM.

Fig.11 indicates that imaging of deeper tissues will decrease contrast. This issue specifies when thermal or random noises are added to the situation; PA signal cannot be distinguished from noise. In addition to Hemoglobin contrast reduction, Fig.12 shows when we go thorough deeper vasculature, the spatial resolution will decrease. In 1.1 mm under surface of head, frequency components of 2.5 MHz can be detected while they can't be resolved in 1.5 mm imaging depth.

V. CONCLUSION

We have demonstrated time-domain and frequency domain analysis of PA signals from various imaging depths, different sizes of hemoglobin absorber containers and various ICG concentrations in vasculature of resting-state mouse brain.

Going deeper through the brain will decrease contrast and resolution of our typical PAM simulated system, something which can be solved by using exogenous contrast agents with greater optical absorption such as ICG.

Comparison of PA signal amplitudes of ICG and Hemoglobin shows a great demand for using various contrast agents in PAM, because, as we discussed, this will increase both spatial or depth resolution and contrast of this microscopic modality.

Simulations and analysis done on different sizes of absorbers in PAM demonstrated that there is a need to ultra-broadband transducers for reaching more precise analysis of PA signals, and this means AR-PAM systems are less efficient for being used in PASA.

REFERENCES

[1] AG. Bell, "On the production of sound by light," Am J Sci., vol. 20, 1880.

[2] Ermilov. SA, Khamapirad. T, Conjusteau. A, Leonard. MH, Lacewell. R, Mehta. K, Miller. T, and Oraevsky. A.," Laser optoacoustic imaging system for detection of breast cancer," J Biomed Opt., vol. 14, 2009.

[3] Wang B, Su JL, Amirian J, Litovsky. SH, Smalling. R, and Emelianov. S.,"Detection of lipid in atherosclerotic vessels using ultrasound-guided spectroscopic intravascular photoacoustic imaging," Opt. Express, vol. 18, pp. 4889–97, 2010.

[4] Wang. X, Ku. G, Wegiel. MA, Bornhop. DJ, Stoica. G, and Wang. LV,"Noninvasive photoacoustic angiography of animal brains in vivo with near-infrared light and an optical contrast agent," Opt. Let., vol. 29, pp. 730-732, 2004.

[5] Ku. G, Zhou. M, Song. S, Huang. Q, Hazle. J, and Li. C,"Copper sulfide nanoparticles as a new class of photoacoustic contrast agent for deep tissue imaging at 1064 nm," ACS. Nano., vol. 6, pp. 7489-7496, 2012.

[6] Su. JL, Bouchard. RR, Karpiouk. AB, Hazle. JD, and Emelianov. SY."Photoacoustic imaging of prostate brachytherapy seeds," Biomed Opt Express., vol. 2, pp. 2243-2254, 2011.

[7] Nie. L, Cai. X, Maslov. K, Garcia-Uribe. A, Anastasio. MA, and Wang. LV. ,"Photoacoustic tomography through a whole adult human skull with a photon recycler," J. Biomed. Opt., vol. 17, pp. 110506-110506, 2012.

[8] Yao. Junjie, Xia. Jun, Maslov. Konstantin. I, Nasiriavanaki Mohammadreza, Tsytsarev Vassiliy, Demchenko. Alexei. V, and Wang. LV.,"Noninvasive photoacoustic computed tomography of mouse brain metabolism in vivo," Neuroimage, Vol. 64, pp. 257-266, 2013.

[9] Yao. Junjie, Wang. Lidai, Yang. Joon-Mo, Maslov. Konstantin.I, Wong Terence. TW, Li. Lei, Huang. Chih-Hsien,Zou. Jun, and Wang. LV.,"High-speed label-free functional photoacoustic microscopy of mouse brain in action," Nature methods, vol. 12, pp. 407-410, 2015.

[10] Tang. Jianbo, Coleman. Jason. E, Dai. Xianjin, and Jiang. Huabei,"Wearable 3-D Photoacoustic Tomography for Functional Brain Imaging in Behaving Rats,"Scientific reports, vol. 6, 2016.

[11] Park. Jongin, Jeon. Seungwan, Meng. Jing, Song. Liang, Lee. Jin S, and Kim. Chulhong,"Delay-multiply-and-sum-based synthetic aperture focusing in photoacoustic microscopy," J. biomed. opt., vol. 21, pp. 036010-036010, 2016.

[12] Feng. Ting, Li. Qiaochu, Zhang. Cheng, Xu. Guan, Guo. L. Jay, Yuan. Jie, and Wang. Xueding,"Characterizing cellular morphology by photoacoustic spectrum analysis with an ultra-broadband optical ultrasonic detector," J. Opt. Exp., vol. 24, pp. 19853-19862, 2016.

[13] Gao. Xiaoxiang, Tao. Chao, Liu. Xiaojun, and Wang. Xueding,"Evaluation of microvasculature diameter in deep tissue using a photoacoustic spectral analysis," Opto-Electronics and Communications Conference (OECC), pp. 1-3, 2015.

[14] R. E. Kumon, C. X. Deng, and X. Wang, "Frequency-domain analysis of photoacoustic imaging data from prostate adenocarcinoma tumors in a murine model," Ultrasound Med. Biol., vol. 37, pp. 834–839, 2011.

[15] Abhinav. K. Jha, M. A. Kupinski, H. H. Barrett, E. Clarkson, and J. H. Hartman,"Three-dimensional Neumann-series approach to model light transport in nonuniform media," J. Opt. Soc. Am. A, Vol. 29, pp. 1885-1899, 2012.

[16] V. Kersemans, J. Thompson, B. Cornelissen, M. Woodcock, P. D. Allen, N. Buls, R. J Muschel, M. A. Hill, and S. C. Smart,"Micro-CT for Anatomic Referencing in PET and SPECT: Radiation Dose, Biologic Damage, and Image Quality," J. Nucl. Med, Vol. 52, pp. 1827-1833, 2011.